

Supplemental Information

**H3K27M in Gliomas Causes a One-Step Decrease
in H3K27 Methylation and Reduced Spreading
within the Constraints of H3K36 Methylation**

Ashot S. Harutyunyan, Haifen Chen, Tianyuan Lu, Cynthia Horth, Hamid Nikbakht, Brian Krug, Caterina Russo, Eric Bareke, Dylan M. Marchione, Mariel Coradin, Benjamin A. Garcia, Nada Jabado, and Jacek Majewski

Table S1 (related to Figures 1-5). List of glioblastoma isogenic cell lines used in the study. WT, wild-type; O/E, overexpression.

Sample name	Diagnosis	Histone mutation	Age	Gender	Location	K27M(+) condition	K27M(-) condition
BT245	GBM	H3.3K27M	8	M	Thalamus	parental	K27M-KO
SU-DIPGXIII	DIPG	H3.3K27M	6	F	Pons	parental	K27M-KO
HSJ019	GBM	H3.3K27M	13	F	Thalamus	parental	K27M-KO
G477	GBM	WT	15	F	Cortex	H3.3K27M O/E	H3.3K27R O/E

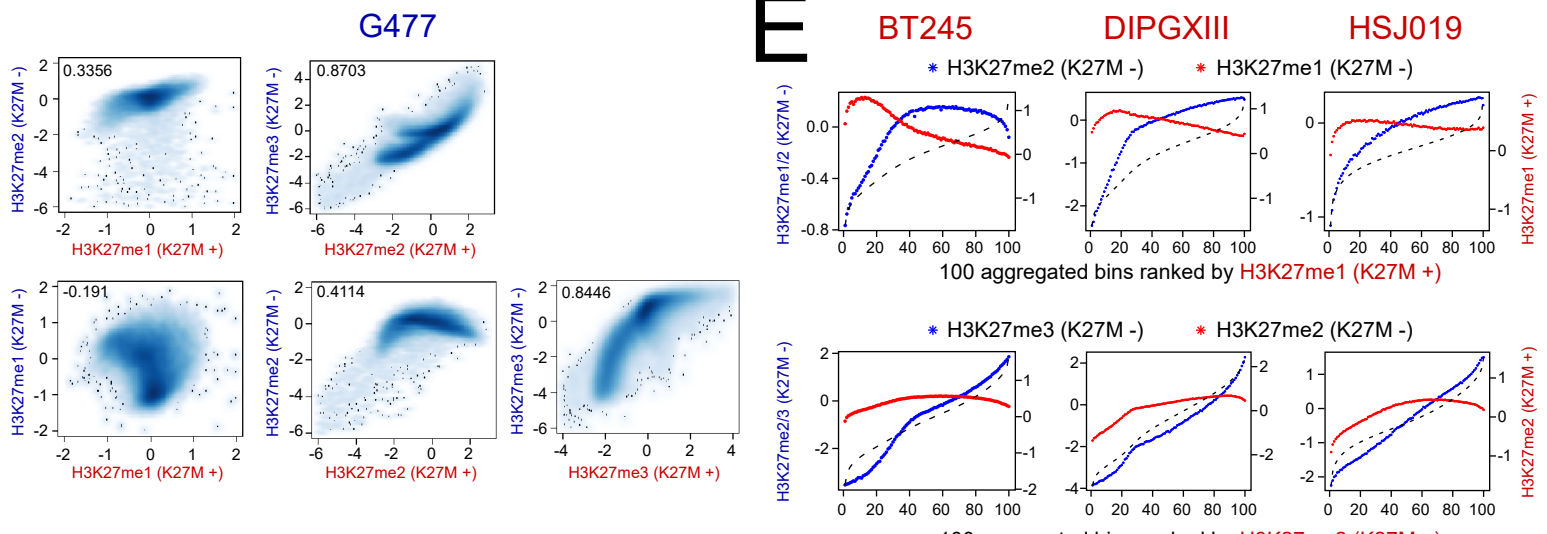
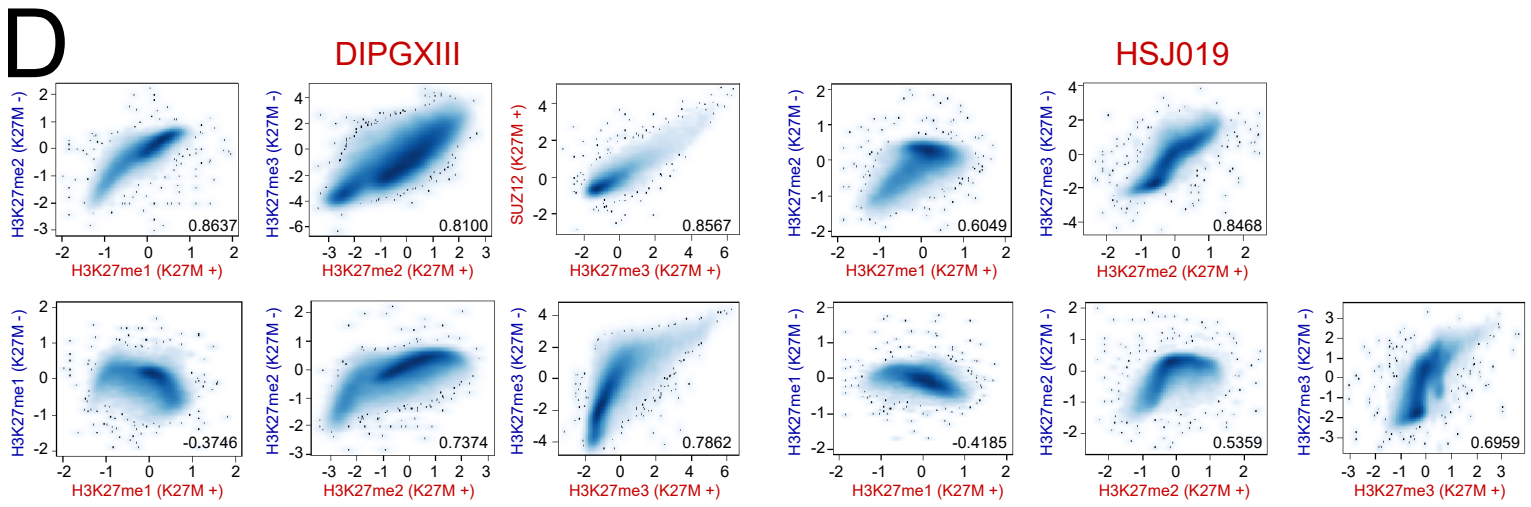
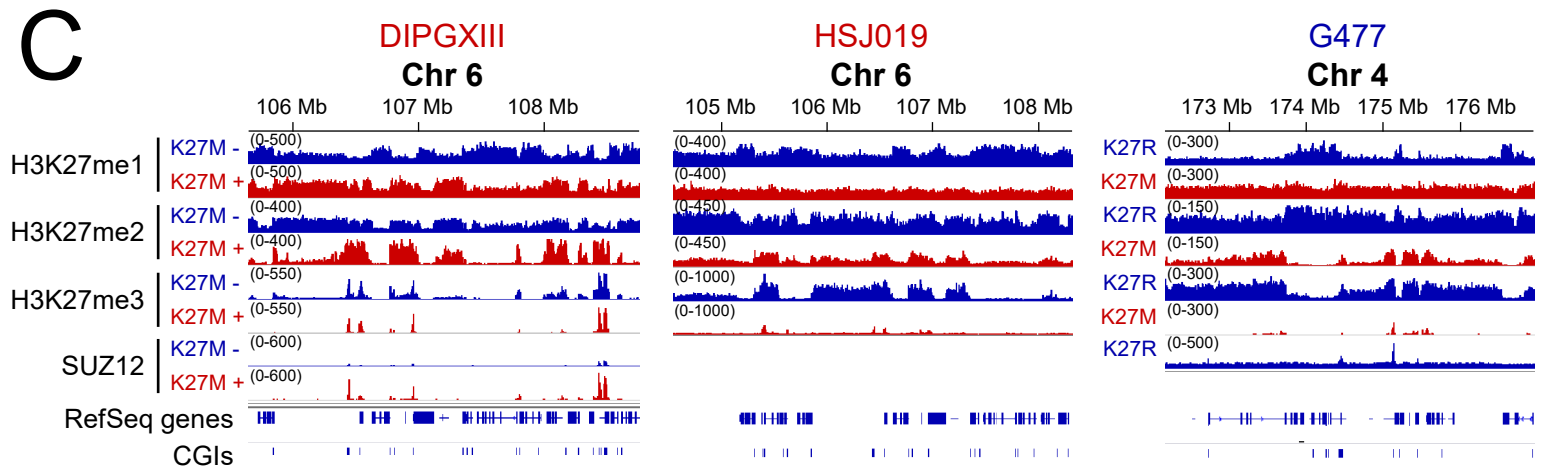
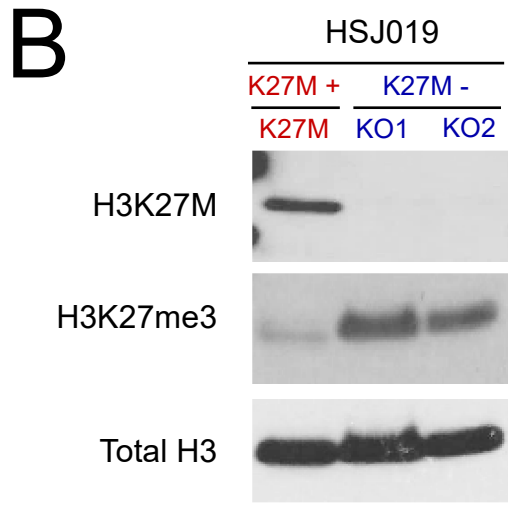
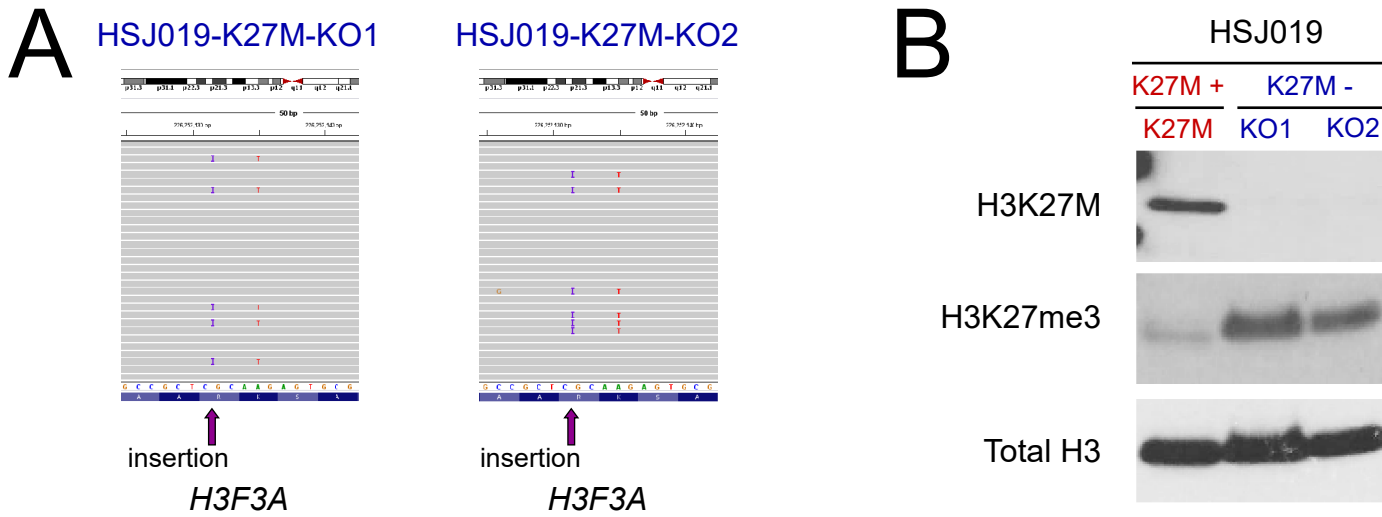


Figure S1 (related to Figure 1). One-step reduction of H3K27 methylation in H3.3 K27M in multiple isogenic cell lines.

(A) MiSeq confirmation of CRISPR editing in HSJ019 cell line.

(B) Western blot showing removal of H3K27M and increase in H3K27me3 levels in HSJ019 cell line. For confirmation of the other cell lines used, please see (Harutyunyan et al., 2019).

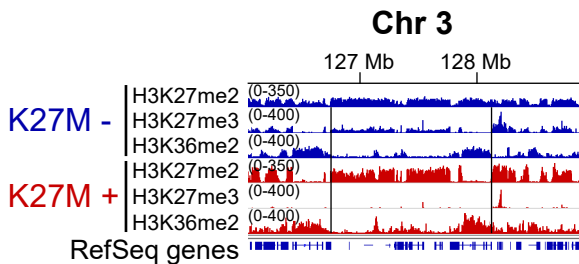
(C) Visualization of ChIP-seq results for H3K27me1/2/3 in DIPGXIII, HSJ019 and G477 K27M (+/-) cell lines.

(D) Genome-wide relationships between different levels of H3K27 methylation in DIPGXIII, HSJ019 and G477, using 100 kb genome-wide bins. H3K27me1 levels in K27M (+) are anticorrelated with those in K27M (-) and more similar to H3K27me2 in K27M (-); H3K27me2 in K27M (+) correlates well with H3K27me3 in K27M (-); high levels of H3K27me3 in K27M (+) correspond to increased levels of SUZ12. Axis scales are log2 (ChIP vs. input), darker color indicates higher density of bins. Total number of bins for DIPGXIII (six panels left to right, up to bottom) – 28241, 28223, 28217, 28241, 28227, 28225, HSJ019 – 28178, 28470, 28181, 28479, 28463, G477 – 28230, 28224, 28211, 28257, 28221. Pearson correlation coefficients are shown in the corners of the plots.

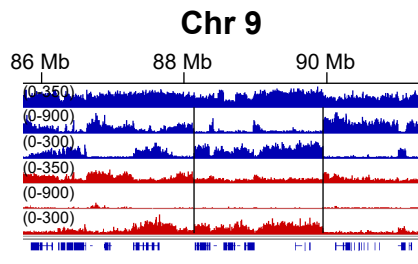
(E) Illustration of relationships between different H3K27 methylation marks using a different approach, as described in previous publications (Baubec et al., 2015; Weinberg et al., 2019): we used 1 kb tiles and aggregated them into 100 bins ranked by the level of H3K27me1/2 in K27M (+).

A

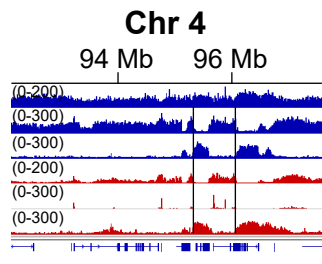
DIPGXIII



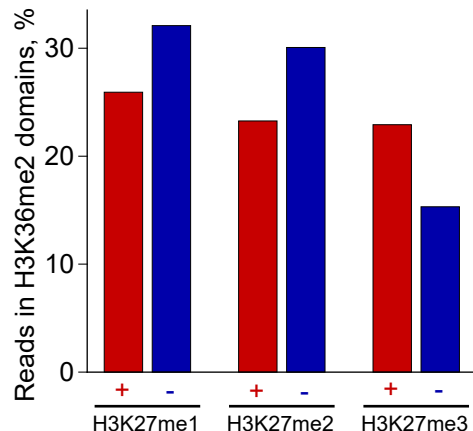
HSJ019



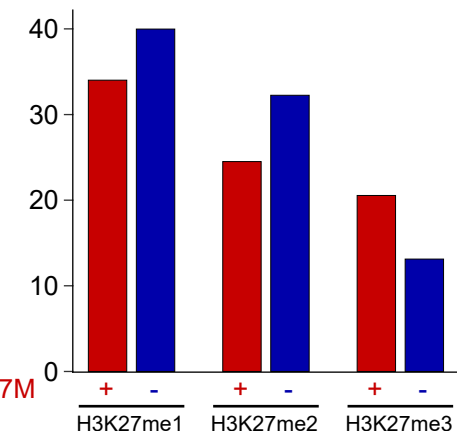
G477

**B**

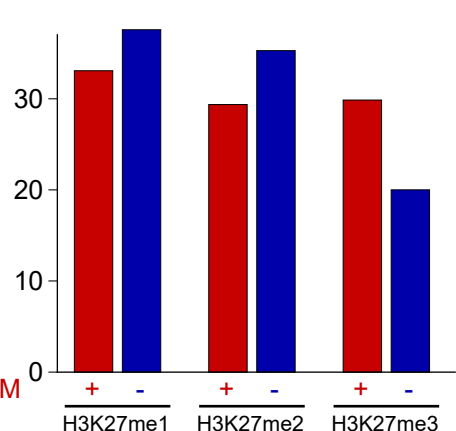
BT245



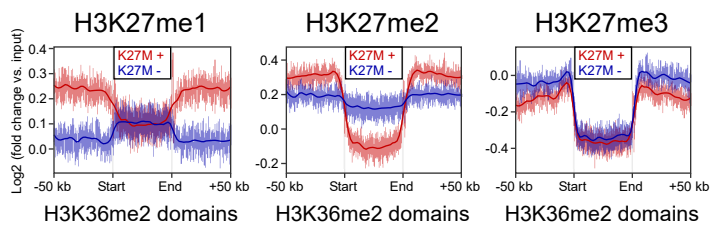
DIPGXIII



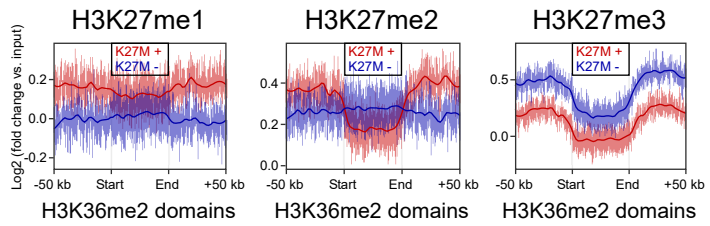
HSJ019

**C**

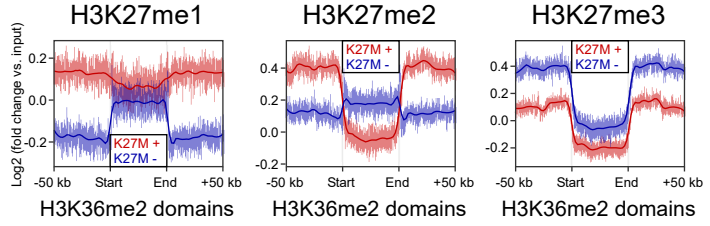
DIPGXIII



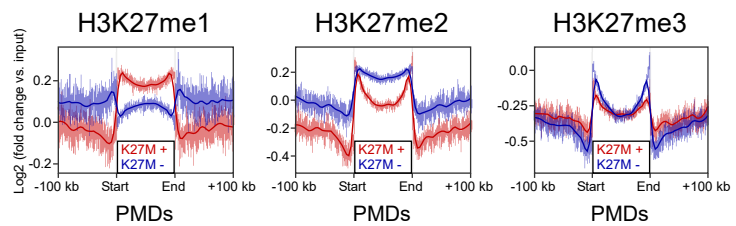
HSJ019



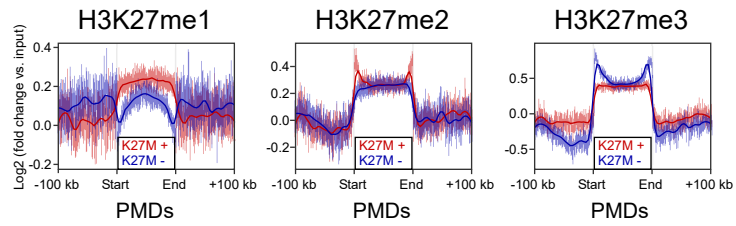
G477

**D**

DIPGXIII



HSJ019



G477

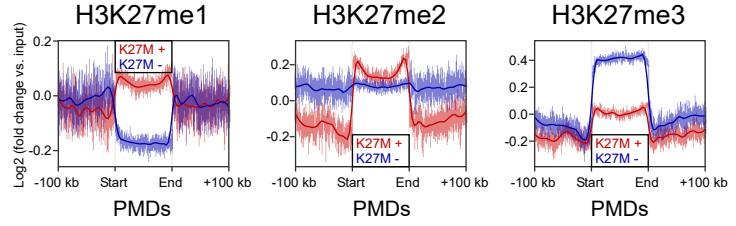


Figure S2 (related to Figure 2). H3K36me2 forms boundaries for H3K27me3 in WT and for H3K27me2 in H3.3 K27M.

- (A)** ChIP-seq tracks showing alternating H3K36me2/H3K27me3 domains in K27M (-) corresponding to alternating H3K36me2/K27me2 domains in K27M (+) in DIPGXIII, HSJ019 and G477 cell lines.
- (B)** Percentage of H3K27me1/me2 reads is decreased in H3K36me2 domains in K27M (+), while H3K27me3 is relatively higher, due to the global loss of H3K27me3 elsewhere.
- (C)** Aggregated signal of H3K27me1/me2/me3 over intergenic H3K36me2 domains in DIPGXIII, HSJ019 and G477 isogenic cell lines. Domains overlapping with H3K36me3 have been removed to exclude its effect.
- (D)** Aggregated signal of H3K27me1/me2/me3 over PMD regions in DIPGXIII, HSJ019 and G477 isogenic cell lines. PMDs represent the most permissive regions for spread of H3K27 methylation in both conditions.

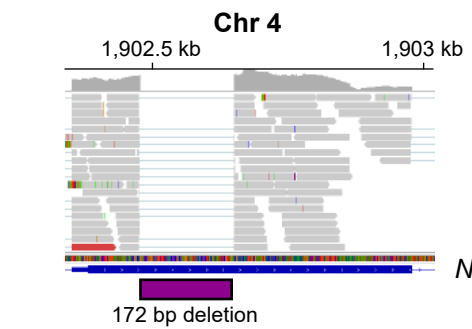
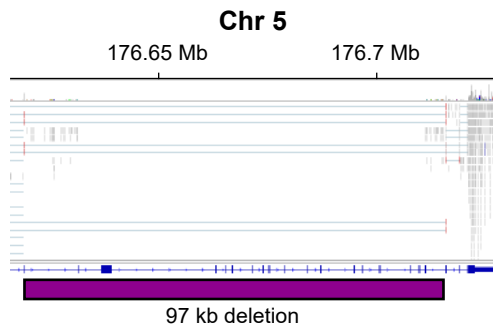
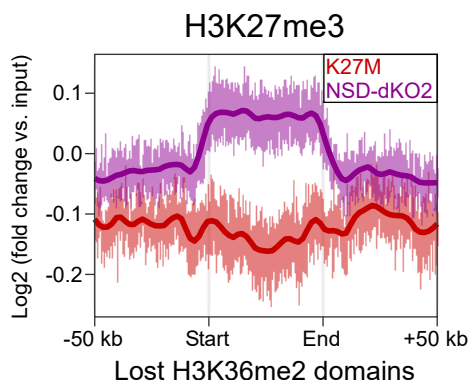
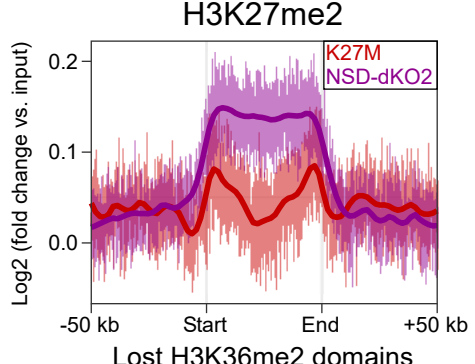
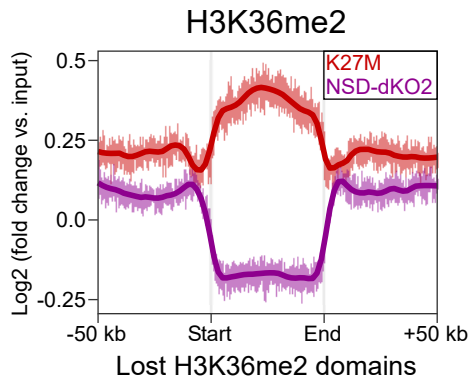
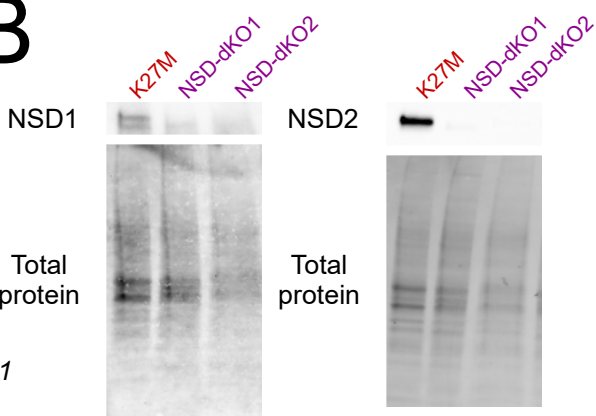
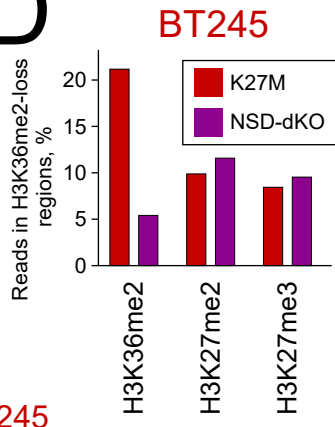
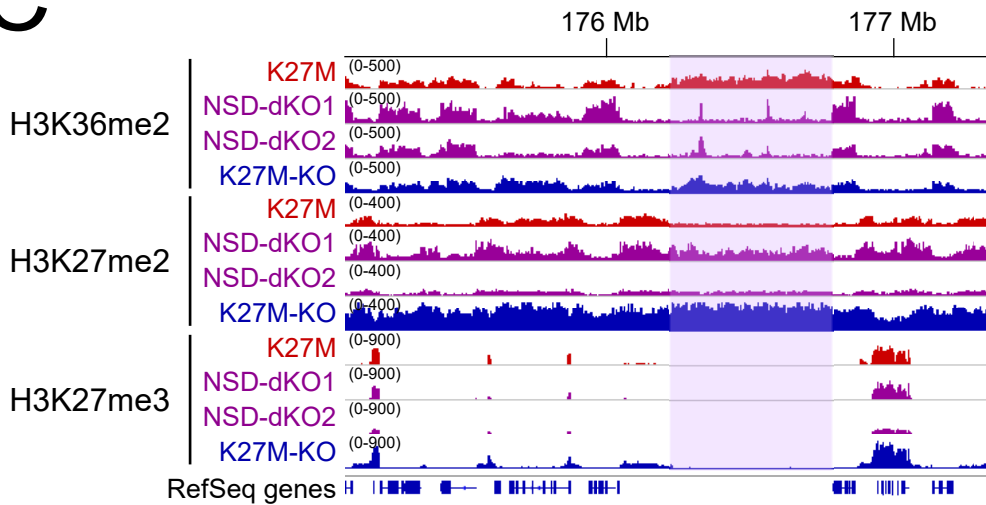
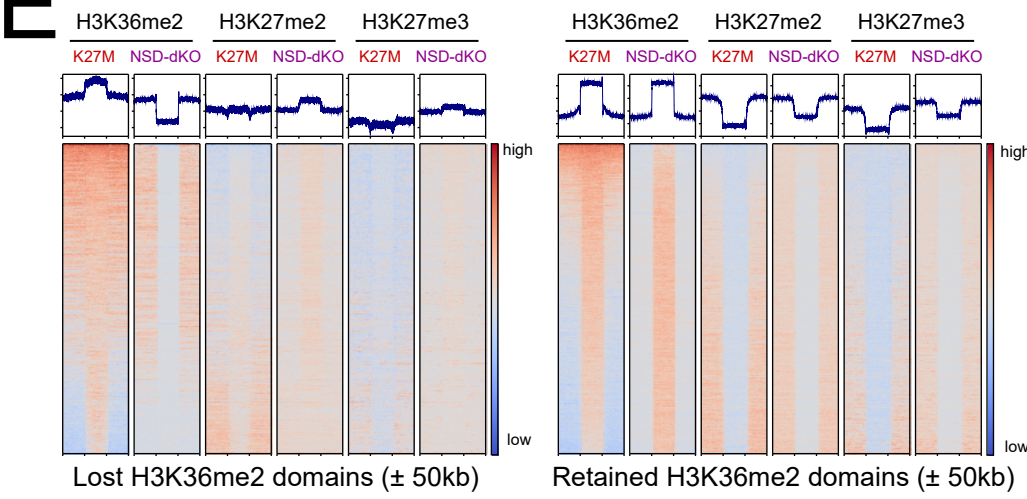
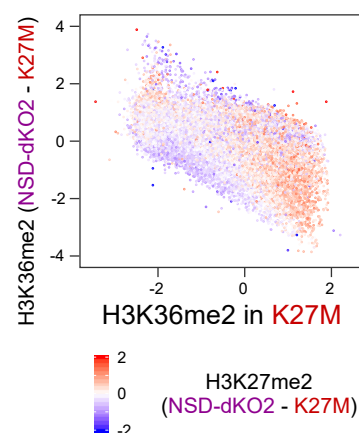
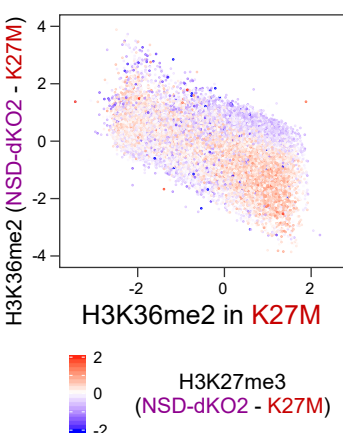
A**BT245-NSD-dKO****F****B****D****C****E****G**

Figure S3 (related to Figure 3). Confirmation of *NSD1/2* CRISPR-KO in BT245 cell line and additional analyses.

- (A)** Confirmation of CRISPR editing in *NSD1* and *NSD2* genes by looking at RNA-seq data (~97kb deletion removing most of *NSD1* and 172bp frameshift deletion in *NSD2*).
- (B)** Western blot showing the absence of NSD1 and NSD2 proteins in NSD1/2-dKO clones of BT245 cell line.
- (C)** ChIP-seq tracks both NSD1/2-dKO clones of BT245 cell line showing H3K27me2/3 spreading into the regions of H3K36me2 loss. Highlighted region illustrates a domain of H3K36me2 loss.
- (D)** Percentage of H3K27me2/me3 reads is increased in the domains of H3K36me2 loss upon NSD1/2-KO.
- (E)** Tornado (heatmap) plots of H3K27me2/3 and H3K36me2 in domains losing H3K36me2 (left panel) and retaining H3K36me2 (right panel) upon NSD1/2-dKO. Increase of H3K27me2/3 is seen only in the regions of H3K36me2 loss.
- (F)** Aggregate signal of H3K36me2 and H3K27me2/3 in the regions of H3K36me2 loss in the second NSD1/2-dKO clone, shows an increase of H3K27me2 and a smaller increase in H3K27me3, similar to the first clone.
- (G)** H3K36me2 signal change in genome-wide 100kb bins of BT245 and NSD1/2-dKO (second clone), color coded by H3K27me3 (left panel) and H3K27me2 (right panel) levels. y axis shows the difference in H3K36me2 levels in K27M vs. NSD1/2-dKO (log2), while x axis shows H3K36me2 levels in K27M. Regions with largest loss of H3K36me2 experience the highest gain of H3K27me2/3 (bottom right).

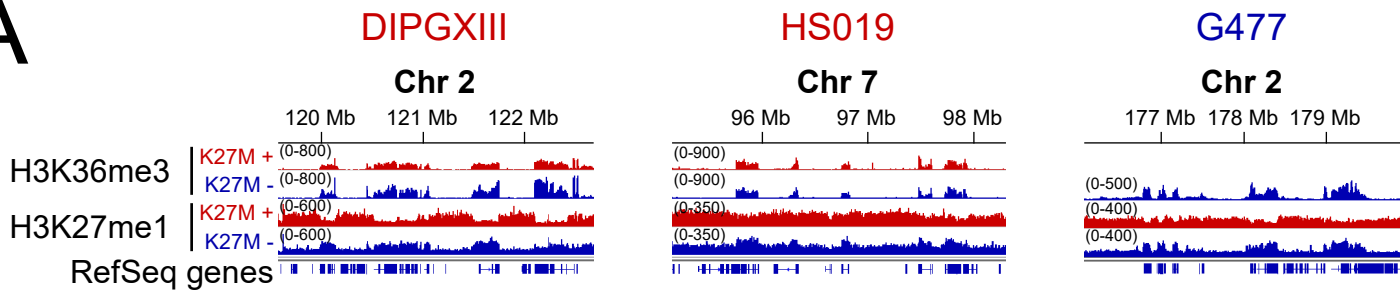
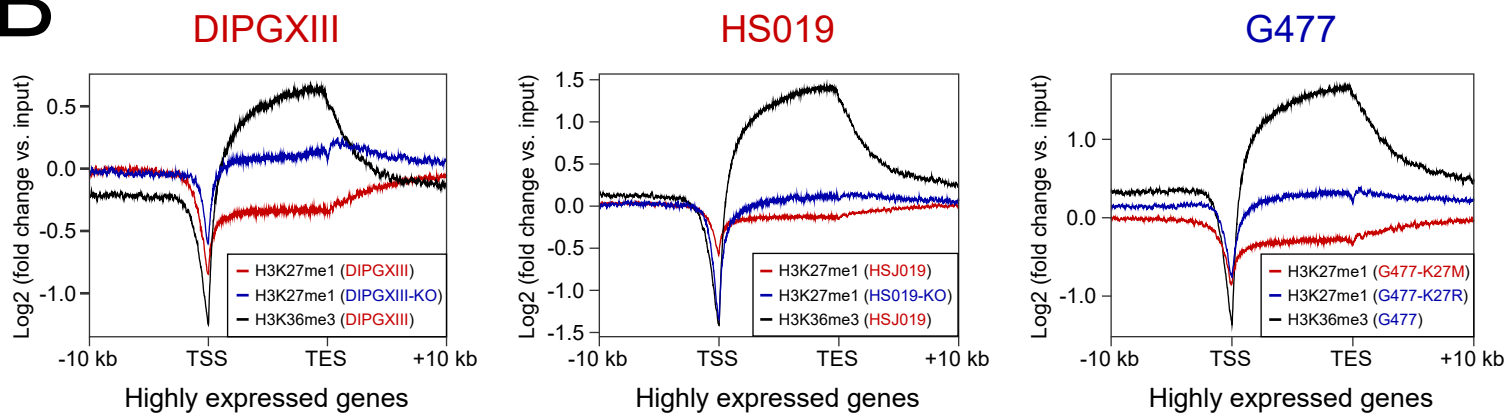
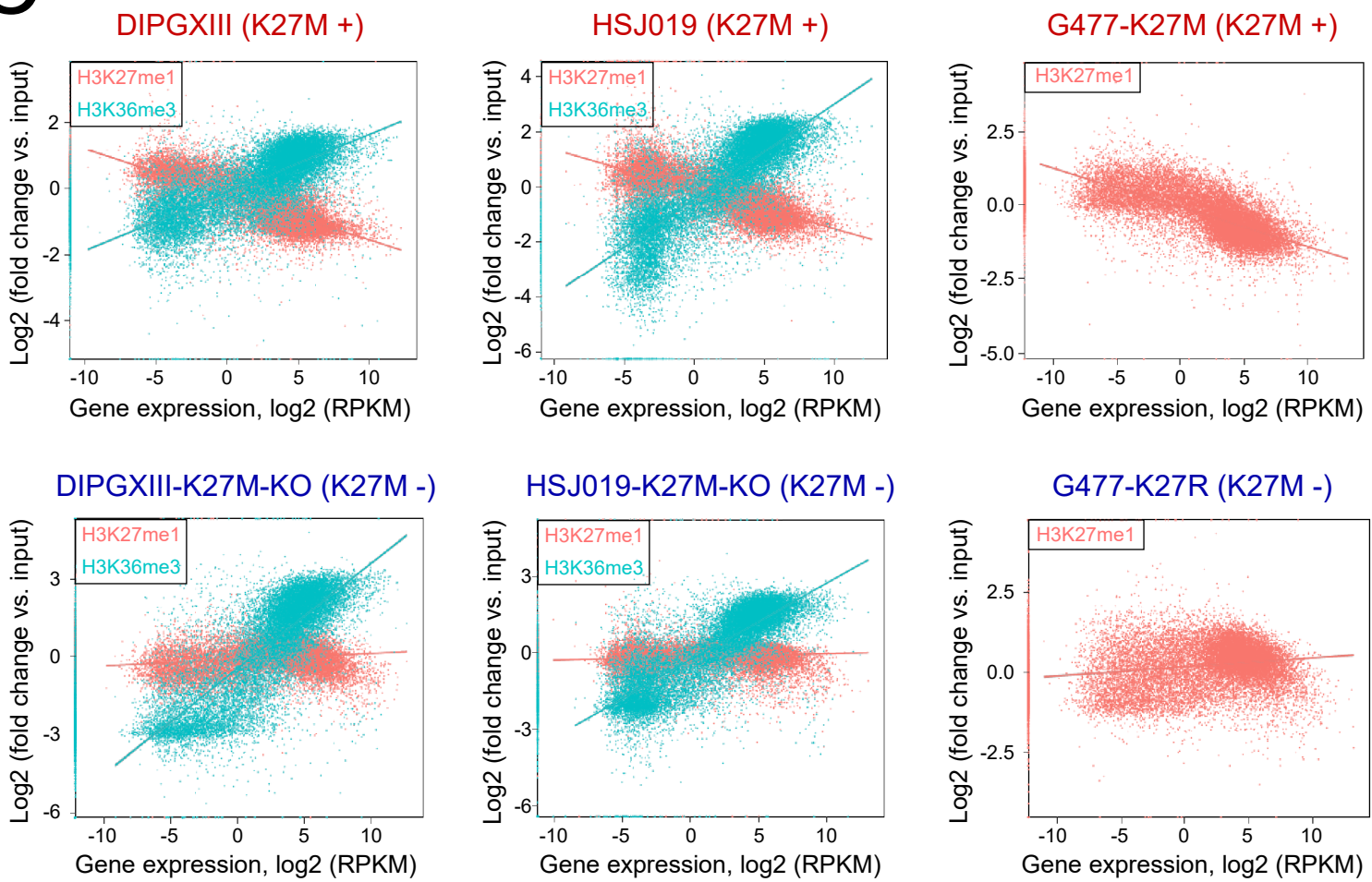
A**B****C**

Figure S4 (related to Figure 4). H3K27me1 association with H3K36me3 and gene expression is absent in H3.3 K27M samples.

(A) ChIP-seq tracks of DIPGXIII, HSJ019 and G477 cell lines showing H3K27me1 domains co-occurring with H3K36me3 in K27M (-), while in K27M (+) H3K27me1 is mainly depleted in H3K26me3-rich regions. No major changes for H3K36me3 are observed.

(B) Aggregate plots of H3K27me1 over genic regions in DIPGXIII, HSJ019, G477.

(C) Correlation plots of H3K27me1 and H3K36me3 signal with gene expression of respective genes. For G477 cell line, H3K36me3 data is not plotted due to the lack of H3K36me3 ChIP-seq data in K27M (+) condition.

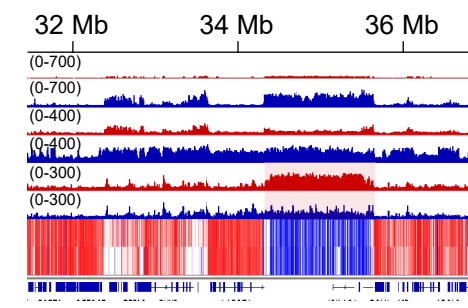
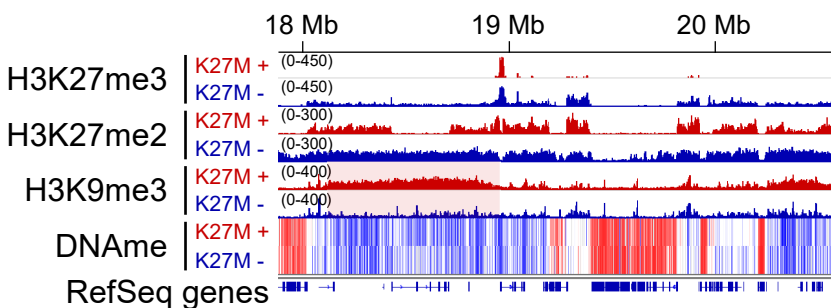
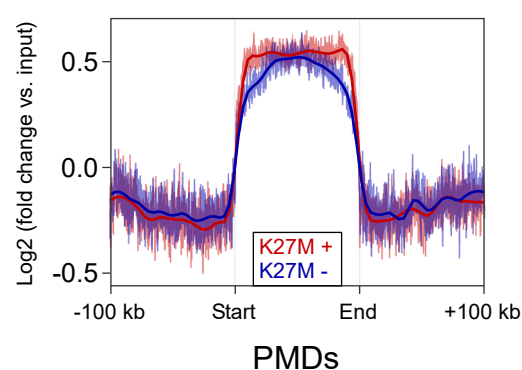
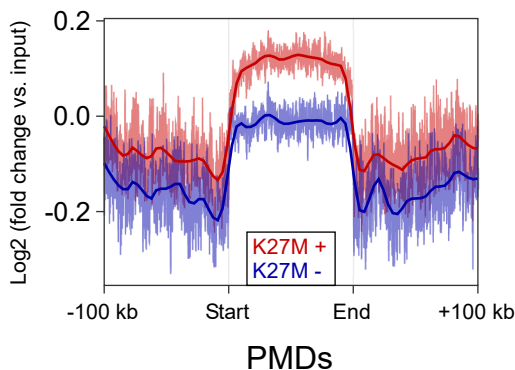
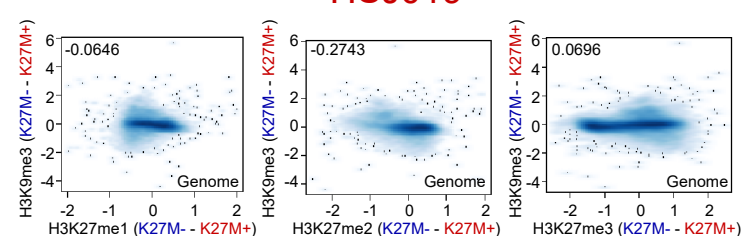
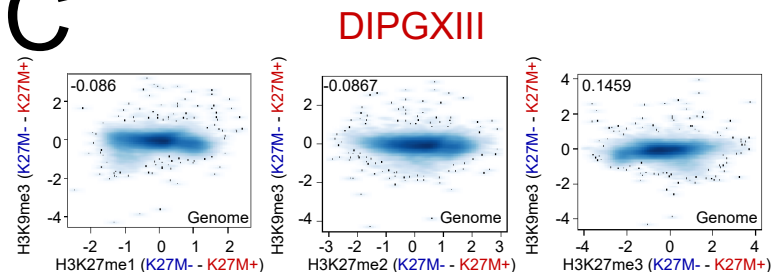
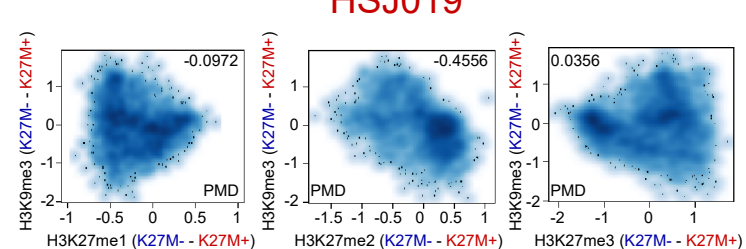
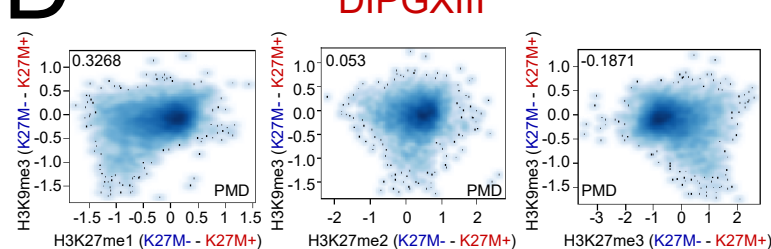
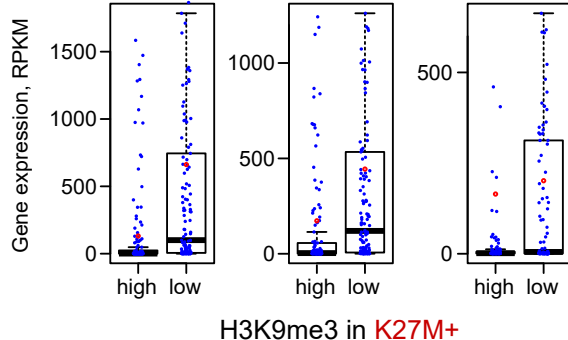
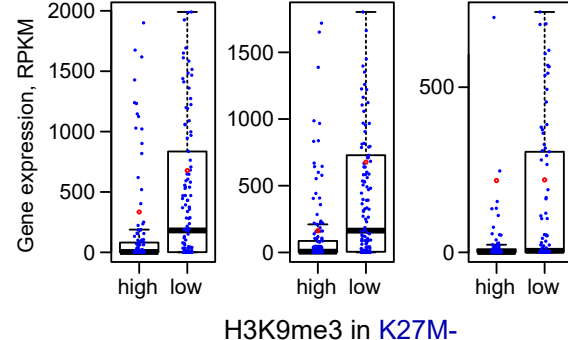
A**DIPGXIII****HSJ019****Chr 1****B****DIPGXIII****HSJ019****C****D****E****BT245****DIPGXIII****HSJ019****BT245****DIPGXIII****HSJ019**

Figure S5 (related to Figure 5). Moderate H3K9me3 increase in domains losing H3K27me2/me3 in H3.3 K27M.

- (A)** ChIP-seq and whole genome bisulphite sequencing tracks showing H3K9me3 enrichment in some H3K27me2-depleted PMDs in DIPGXIII and HSJ019 cell lines.
- (B)** Aggregate plots of H3K9me3 over PMDs, summarizing the observed changes on ChIP-seq tracks in DIPGXIII and HSJ019.
- (C-D)** Correlation plots of H3K9me3 change with changes in H3K27me1/me2/me3 marks genome-wide **(C)** and in PMD regions **(D)**. Pearson correlation coefficients are shown in the corners of the plots.
- (E)** Box plots of gene expression levels for genes in PMD regions with low and high levels of H3K9me3. Gene expression is higher in the regions with low H3K9me3. Numbers in brackets above the plots show average RPKM level for each group.